Biomaterials 35 (2014) 8357–8373

Contents lists available at ScienceDirect

Biomaterials

journal homepage: www.elsevier.com/locate/biomaterials

Pluronic-encapsulated natural chlorophyll nanocomposites for *in vivo* cancer imaging and photothermal/photodynamic therapies

Maoquan Chu [a, b, *], Haikuo Li [c], Qiang Wu [a], Fangjie Wo [a], Donglu Shi [d, e]

[a] School of Life Science and Technology, Tongji University, Shanghai 200092, PR China
[b] Research Center for Translational Medicine at Shanghai East Hospital, Tongji University, 150 Jimo Road, Shanghai 200120, PR China
[c] Shanghai Institute of Applied Physics, Chinese Academy Science, Shanghai 201800, PR China
[d] The Institute for Biomedical Engineering & Nano Science, Tongji University School of Medicine, Shanghai 200092, PR China
[e] The Materials Science and Engineering Program, Dept of Mechanical and Materials Engineering, College of Engineering and Applied Science, University of Cincinnati, Cincinnati, OH 45221-0072, USA

ARTICLE INFO

Article history:
Received 14 May 2014
Accepted 17 May 2014
Available online 4 July 2014

Keywords:
Dietary chlorophyll
Organic nanocomposites
In vivo cancer imaging
Photothermal therapy
Photodynamic therapy

ABSTRACT

A great challenge in developing nanotechnologies for cancer diagnosis and therapy has been the combined functionalities required for complicated clinical procedures. Among all requirements, toxicity has been the major hurdle that has prevented most of the nano-carriers from clinical use. Here, we extracted chlorophyll (Chl) from vegetable and encapsulated it into polymer (pluronic F68, Plu) micelles for cancer imaging and therapy. The results showed that the Chl-containing nanocomposites were capable of mouse tumor targeting, and the nanocomposite fluorescence within the tumor sites remained at high intensity more than two days after tail-vein injection. It is interesting that oral administration with the nanocomposites was also successful for tumor target imaging. Furthermore, the dietary Chl was found to be able to efficiently convert near-infrared laser irradiation to heat. The growths of melanoma cells and mouse tumors were effectively inhibited after being treated with the nanocomposites and irradiation. The suppression of the tumors was achieved by laser-triggered photothermal and photodynamic synergistic effects of Chl. As a natural substance from vegetable, Chl is non-toxic, making it an ideal nanocarrier for cancer diagnosis and treatment. Based on the results of this research, the Plu–Chl nanocomposites have shown promise for future clinical applications.

1. Introduction

Cancer remains one of the world's most devastating diseases [1]. The current challenges in effective cancer treatment lie on finding novel approaches for early cancer diagnosis and targeted therapy. The delivery of drug or other therapeutic means, be it chemical or physical, has to be targeted and navigated to the tumor site with high specificity. The delivery system is also required to be low or non toxic. Therefore, searching for a carrier system in cancer diagnosis and therapy has been the main activities in the research fields. Although a variety material has been identified, none can entirely meet all biomedical, especially clinical requirements. Natural chlorophyll (Chl) may be an ideal candidate in cancer-target imaging and therapy for its non-toxicity and abundance in nature. Other photo-thermal properties further qualify it as an effective therapeutic material.

Natural Chl absorbs sunlight, which can be used in photosynthesis. This process is commonly observed in plants, algae, and cyanobacteria. Chl is also responsible for the green color of these organisms. The molecular structure of Chl is similar to that of the near-infrared (NIR) fluorescent porphyrin. NIR fluorescence is preferred for *in vivo* fluorescent imaging for its deeper penetration depth in the animal tissues. Chl was previously used for animal sentinel lymph node mapping in our work [2]. Chl and its various derivatives were also used for cancer prevention [3,4]. Since Chl has the structure of conjugated macrocyclic ligand, Chl has been used as a photosensitizer for cancer photodynamic therapy (PDT) [5–9]. The first PDT usage of a chlorin relates to a pheophorbide a derivative [8]. Now several Chl derivatives such as talaporfin sodium, photochlor and padachlorin have been entered clinical trials for PDT [5-7]. In this research, the photothermal effect of Chl was discovered and investigated in vitro and *in vivo* for cancer photothermal therapy (PTT).

* Corresponding author. School of Life Science and Technology, Tongji University, Shanghai 200092, PR China.
E-mail address: mqchu98@tongji.edu.cn (M. Chu).

http://dx.doi.org/10.1016/j.biomaterials.2014.05.049
0142-9612/

Chl used in this work was extracted from cabbage mustard. Cabbage mustard is one of the most common vegetables used in daily food consumption. The polymer micelles formed by pluronic F68 (abbreviated as Plu) was used to encapsulate Chl for improved water solubility. Plu is a linear molecule consisting of a central hydrophobic polypropylene oxide region that is flanked on either side by hydrophilic polyethylene oxide domains of equal length. This amphiphilic block copolymer has been approved by Federal Drug Administration for intravenous administration. The Plu-encapsulated Chl (Plu–Chl) nanocomposites without any antibody or peptide conjugation were investigated for cancer target imaging. The procedure was carried out via tail vein injection or gavage. Also investigated was the photothermal conversion of the Plu–Chl nanocomposites upon laser irradiation for PTT of cancer. We used melanoma-beared mice for these studies since this skin cancer has the fastest rising incidence of any malignancy in the Western world [10].

In our previous study [11], fluorescent quantum dots (QDs) were found to exhibit highly efficient photothermal effect that completely inhibited mouse tumor growth using the PTT strategy. However, the toxicity of QDs has been a major concern in medical therapy. Other bifunctional inorganic nanoparticles such as gold nanostructures [12,13], graphene [14], and magnetic gold nanocomposites [15], although have been widely investigated for both imaging and cancer phototherapy, present similar concerns in clinical trials. The major advantage of natural Chl lies in its biosafety for which it is an important nutrition in our daily diets and has been used in traditional medicine [16]. Therefore, Chl-based nanocomposites may serve as the ideal and promising carrier system in cancer diagnosis and therapy.

2. Materials and methods

2.1. Materials

2.1.1. Reagents and materials

Fresh cabbage mustard plants were purchased from a local food market (Shanghai, China). Plu was purchased from Sigma–Aldrich Corporation. Methanol, ethanol, petroleum ether (b.p. 30–60 °C) were purchased from Sinopharm Chemical Reagent Co., Ltd. (Shanghai, China).

The RPMI-1640 culture medium and fetal bovine serum (FBS) were obtained from Gibco (Carlsbad, CA, USA). 2,7-Dichlorodihydrofluorescein diacetate (DCFH-DA), hematoxylin and eosin (H&E) staining kit and terminal deoxynucleotidyl transferase (TdT)-mediated dUTP nick end labeling (TUNEL) kit were was purchased from Beyotime Institute of Biotechnology (Jiangsu, China). CellTiter-Glo® luminescent cell viability assay reagents were purchased from Promega Corporation (Madison, WI, USA).

2.1.2. Cell lines and animal model

Human A375 melanoma cells were purchased from the Shanghai Institute for Biological Sciences, Chinese Academy of Sciences (Shanghai, China). Nude BALB/c mice aged 6–7 weeks were purchased from the Shanghai Sipper-BK Lab Animal Co., Ltd. (Shanghai, China), and were used in accordance with approved institutional protocols established by the Shanghai Department of Experimental Animals Management. All mice were housed in positive-pressure air-conditioned units (25 °C, 50% relative humidity) on a 12-h light, 12-h dark cycle, in a specific pathogen-free (SPF) environment.

2.2. Methods

2.2.1. Preparation of Plu-coated Chl nanocomposites

The methods of detecting the distribution of Chl in cabbage mustard plants and extraction of Chl were shown in the Supporting Information. For a typical experiment of the preparation of Plu–Chl nanocomposites, Chl (10 mg) and Plu (10 mg) were dissolved in chloroform (2 mL) in a round-bottomed flask, and dried via rotary evaporation to make a thin film. The film was then blown dry with nitrogen to remove any residual chloroform. Phosphate buffered saline (PBS) (1 mL) was added to the flask, gently shaken for at least 30 min, and then sonicated for 15–20 min. Immediately after sonication, the solution was stored at 4 °C under dark condition. For the preparation of Plu-coated Chl nanocomposites with different mass ratios (4:1, 2:1, 1:2, and 1:4) of Plu to Chl, or the preparation of nanocomposites containing different concentrations of Chl or FBS-dispersed nanocomposites, the method described above was applied, and only the amount of Chl or the solvent type was changed.

2.2.2. Measurements of the morphology and size distribution of the Plu–Chl nanocomposites

The morphologies and energy dispersive X-ray spectrometry (EDS) spectra were investigated using a high-resolution transmission electron microscope (HRTEM) (JEOL-2010, Japan) operating at 200 kV. The size distribution was determined using the photon correlation spectroscopy (PCS) (3000HS, Malvern). Before the size measurements, the solutions were extruded through a polycarbonate membrane filter (Sinopharm Chemical Reagent Co., Ltd) with pore diameters of 0.8 μm.

2.2.3. Absorption and fluorescent emission spectra, and stability assay of the Plu–Chl nanocomposite

The absorption spectra of the Plu-Chl nanocomposites were measured using a diode-array spectrophotometer (UV-2102PC, Unico, Shanghai, China) with a deuterium lamp source. The fluorescence spectra were measured using a fluorescence spectrometer (F-2500, Hitachi, Japan) with a xenon lamp source. To investigate the fluorescence stability of the Plu–Chl nanocomposites in PBS and 100% FBS, the PBS- and FBS-dispersed nanocomposite solutions containing 0.05 mg/mL of Chl and 0.05 mg/mL of Plu were immersed in a thermostat water bath, which was maintained at 37 °C. The fluorescence spectra of the samples were measured after being heated for 5, 48, 72, 96, 120, and 144 h. For each kind of solution, it was divided into 18 solutions (1 mL for each tube). Three arbitrary tubes were taken out from the thermostat water bath at each time point for fluorescence detection. Excitation wavelength was 400 nm.

2.2.4. Fluorescence imaging of Plu–Chl nanocomposites

Brightfield images of Plu–Chl nanocomposites dispersed in PBS and FBS and exposed to a daylight lamp were recorded using a digital color camera. Fluorescence images of the PBS- and FBS-dispersed nanocomposite solutions were obtained using the *in vivo* imaging system (NightOWL II LB 983 NC100: Berthold Technologies GmbH & Co. KG, Bad Wildbad, Schwarzwald, Germany). The fluorescence excitation and emission filters were at 630 and 700 nm, respectively. The exposure time was 0.1 s. The mass ratio of the Plu to Chl was maintained at 1:1 in the nanocomposites. The concentrations of Chl in the solutions were 0, 0.036, 0.078, 0.156, 0.313, 0.625, 1.25, and 2.5 mg/mL.

2.2.5. Uptake of Plu–Chl nanocomposites by cancer cells

The A375 cells (~1×10^4 cells) were incubated with 200 μL of RPMI-1640 medium-dispersed Plu–Chl nanocomposites (Chl = Plu = 0.5 mg/mL) at 37 °C for 0.5, 6, and 55 h. After the incubation was completed, the culture medium was removed, and the cells were gently washed several times with PBS, and then imaged using a laser-scanning confocal fluorescent microscope (TCS NT: Leica, Nussloch,Germany). In order to pinpoint the whereabouts of the fluorescent nanocomposites in cells, sequential optical sections were taken along the horizontal section of the cells using the confocal fluorescent microscope. The excitation wavelength was 488 nm, and the emission filter was 600–750 nm.

2.2.6. In vivo tumor targeting, monitored using NIR fluorescence imaging

2.2.6.1. Injection with the Plu–Chl nanocomposites, via tail veins. Three mice were injected subcutaneously with human melanoma cells (~1×10^6 A375 ells). After the tumor size reached 5–10 mm, the tumors were resected and sectioned into pieces (~1×1 mm) and then implanted into at least 90 mice.

The mouse tumors in the size range from 6 to 10 mm were selected for subsequent *in vivo* fluorescent imaging. For a typical experiment, a tumor-bearing mouse was anaesthetized using 4% chloral hydrate, and the PBS-dispersed Plu–Chl nanocomposites (200 μL, Chl = Plu = 10 mg/mL) were then injected into the mouse via the tail vein. The *in vivo* fluorescent images were taken using the *in vivo* imaging system. The excitation and emission filters were 630 and 700 nm, respectively. The exposure time was 0.1 s. The fluorescence was monitored for more than 55 h after injection.

To directly observe the mouse organ and tumor fluorescence at different times after injection, nine tumor-bearing mice were killed at 6, 30, and 55 h post-injection (three mice for each time). As a control, three tumor-bearing mice that had not been injected were also killed, and their tumors and organs were resected. The mouse tumors and organs—including hearts, lives, spleens, lungs, kidneys—were resected and imaged. The imaging method was the same as that described above. To ensure that the mice were killed at the same time (*e.g.* 6 h after injection), only four mice (including a control mouse) were injected with the Plu–Chl and then killed at 6, 30, and 55 h post-injection, respectively. Therefore, these animal experiments were performed three times.

2.2.6.2. Treatment with the Plu–Chl nanocomposites via intragastric administration

In a typical experiment, a tumor-bearing mouse was gavaged with 0.5 mL of PBS-dispersed Plu–Chl nanocomposites (Chl = Plu = 10 mg/mL), and *in vivo* images were taken at different times after the intragastric administration, using the same method as that described above. The fluorescence was monitored for more than 72 h after the intragastric administration.

In addition, fifteen tumor-bearing mice were also gavaged with the nanocomposites (Chl = Plu = 10 mg/mL, 0.5 mL for each mouse) via intragastric

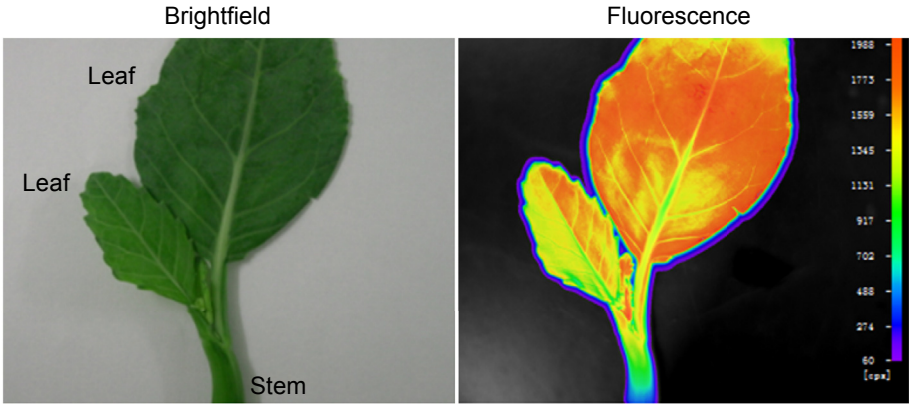

Fig. 1. Brightfield and corresponding fluorescence images of a cabbage mustard plant.

administration, and these mice were killed at different times (3, 8, 24, 72, 168 h) (three mice for each time) after the intragastric administration. As a control, three tumor-bearing mice that were not subjected to intragastric administration were also killed. All of the mouse organs and tumors were then synchronously imaged.

The average fluorescence intensities of each organ and tumor were analyzed using the software provided with the *in vivo* imaging system.

2.2.7. Measurement of the temperature increase in Plu–Chl nanocomposites under 671-nm laser irradiation

A Plu–Chl aqueous solution (Plu = Chl = 8 mg) was dropped on a Parafilm (thickness: 127 μm, melting point: 68 °C)(PM-996, Parafilm, WI, USA), dried naturally and then irradiated by a 671-nm laser (Shanghai Inter-Diff Optoelectronics Technology Co., Ltd., Shanghai, China) (power density: 0.2 W/cm^2, spot area: 9 × 9 mm). As a control, the Parafilm was covered with 8 mg of Plu alone and irradiated with the same laser as described above.

The temperature measurements of the Plu–Chl aqueous solutions were performed in the same manner as those described in our previous work [17]. Briefly, 200 μL of PBS-dispersed Plu–Chl nanocomposites (Chl:Plu = 1:1 wt/wt) were placed in glass tubes (inner diameter, 6 mm) and the open ends of the tubes were covered with sealing film after the solutions were added. A chromel-alumel thermocouple thermometer (Shanghai Instrument Factory Co., Ltd., Shanghai, China) equipped with a probe (0.25 mm in diameter) was used for the temperature measurements. The original temperature was maintained at 25.1 ± 0.1 °C. The 671-nm laser was used to irradiate the solutions for 0–20 min. After irradiation for each time period was completed, the laser was blocked, and the probe was immediately inserted into the solutions. To provide a control, the temperature of 200 μL of PBS and PBS-dispersed Plu solutions under 671-nm laser irradiation was measured using the same method as that described above. The temperature change in each type of sample was measured three times.

2.2.8. Assay of intracellular reactive oxygen species (ROS) produced by the Plu–Chl nanocomposites

The method of the ROS detection was similar with that described in our previous work [11,17], and the details were shown in the Supporting Information.

2.2.9. Cell viability assay

Dead adherent cells typically exhibit significant crimping, deformation, or disintegration, which can be observed clearly using a microscope. Therefore, we used a fluorescent microscope (ECLIPSE TE2000-S, Nikon, Japan) to analyze the state of the cells after they were treated using the photothermal and photodynamic effects of the Plu–Chl nanocomposites. The A375 cells were seeded into 96-well plates (~1 × 10^4 cells) and incubated with 200 μL of RPMI-1640 medium-dispersed Plu–Chl nanocomposites (Chl = Plu = 0.5 mg/mL). The cells were irradiated with the 671-nm laser for 20 min, and then continuously cultured at 37 °C for 1 h. The state of the cells incubated with Chl (0.5 mg/mL, without Plu) and subjected to 20 min of laser irradiation—as well as the state of the cells alone, with and without 20 min of laser irradiation—were also imaged. The excitation wavelength was 488 nm.

The quantitative detection method used to determine the cell viability was similar with that described in our previous work [17]. Briefly, the cells were seeded in 96-well plates (~1 × 10^4 cells, 100 μL in each well, only three wells of each 96-well plate were used) and cultured at 37 °C. The medium was then removed, and 100 μL of medium-dispersed Plu–Chl nanocomposites were then added to two wells, and 100 μL of culture medium alone (as a control) was added to the other well. One of the wells containing Chl was irradiated for 20 min using the 671- nm laser. After irradiation, the cells were continuously cultured at 37 °C for 1 h. The cell viabilities were then measured using the CellTiter-Glo reagent. The mass ratio of Plu to Chl in the nanocomposites was maintained at 1:1, and the concentrations of Chl in the mediums were 0.05, 0.15 and 0.5 mg/mL. In addition, the viabilities of the cells incubated with Chl (0.5 mg/mL) but no Plu, with and without laser irradiation, were also measured.

2.2.10. Mouse tumor retention of the Plu–Chl nanocomposites

70 μL of PBS-dispersed Plu–Chl nanocomposites (Chl = Plu = 5 mg/mL) were intratumorally injected into one mouse tumor (length ≈ width ≈ 5 mm), and the change of tumor fluorescence was then monitored using the *in vivo* imaging system.

In addition, other six tumor-bearing mice were intratumorally injected with 70 μL of PBS-dispersed Plu–Chl nanocomposites (Plu = Chl = 5 mg/mL) and three tumor-bearing mice were intratumorally injected with 70 μL of PBS-dispersed Plu (Plu = 5 mg/mL). The mice in Plu–Chl group were killed at 5 h and 27 h post-injection (three mice for each time), respectively. The mice in Plu group were killed at 5 h post-injection as well. The tumors and the organs including heart, liver, spleen, lung and kidney were resected and their fluorescent images were taken using the *in vivo* imaging system. The imaging method was the same as that described above.

2.2.11. Phototherapy in tumor-bearing mice

2.2.11.1. Intratumoral injection and laser irradiation. Tumor-bearing mice with similar sized tumors (length ≈ width ≈ 5–6 mm) were selected for the photothermal therapy. PBS-dispersed Plu–Chl nanocomposites (Chl = Plu = 5 mg/mL) and

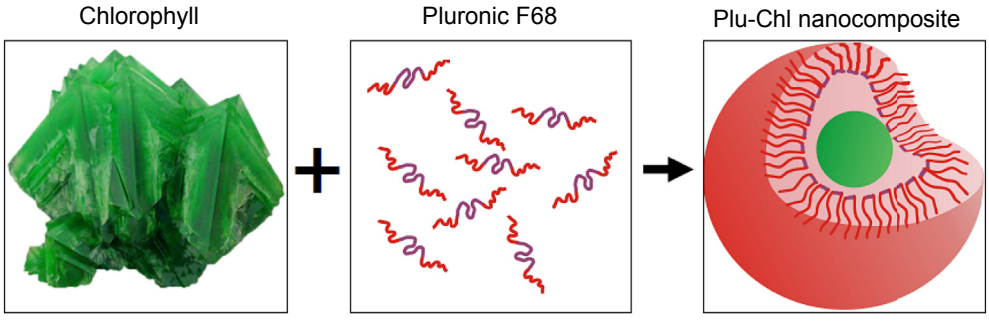

Fig. 2. Schematic illustration of formation of the Plu–Chl nanocomposites.

Plu alone (5 mg/mL) were intratumorally injected into mouse tumors ($n = 10$ for Plu–Chl; $n = 4$ for Plu) every three days. Each mouse was injected three times (70 μL for each time). After the first set of injections were finished, the mice injected with Plu and one group of mice injected with Plu–Chl ($n = 5$) was irradiated with the 671-nm laser for 20 min every 24 h. For these irradiation groups, the irradiation was performed at approximately 5 h after each injection. The tumors were continuously irradiated for 21 days. The other group of mice injected with Plu–Chl ($n = 5$) was not irradiated with the laser.

2.2.11.2. Tail vein injection and laser irradiation. The tumor-bearing mice ($n = 4$) were injected with 200 μL of PBS-dispersed Plu–Chl nanocomposites (Chl = Plu = 10 mg/mL) every three days, via their tail veins. Each mouse was injected three times. At approximately 6 h after the first injection, each mouse was irradiated with the 671-nm laser for 20 min; this was performed every 24 h. All of the tumors were subjected to this irradiation over a period of 21 days.

2.2.11.3. Intragastric administration and laser irradiation. The mice ($n = 4$) were fed with the Plu–Chl nanocomposites (Chl = Plu = 10 mg/mL) every 24 h for 20 days (0.5 mL for each mouse and each time), via intragastric administration. The tumors were irradiated with the 671-nm laser every 24 h, over a period of 21 days.

As a control, a group of tumor-bearing mice ($n = 4$) were not treated with the Chl, and were not irradiated with the laser.

We used a digital color camera to record the tumor morphologies during the treatment. The tumor sizes were measured at the widest point (width), and perpendicular to the longest dimension (length). The tumor volumes were calculated based on the expression $V = L \times W^2/2$. In this equation, V, L, and W are the tumor volume, length, and width, respectively. When the tumors disappeared, the tumor volumes were recorded as zero.

2.2.12. Histological analysis

Two tumor-bearing mice were intratumorally injected with 70 μL of PBS-dispersed Plu–Chl nanocomposites (Chl = Plu = 5 mg/mL). One tumor was irradiated with the 671-nm laser for 20 min every 24 h. Another tumor was not irradiated. Three days after injection, the mice were anesthetized with an intraperitoneal injection of chloral hydrate (4%). The tumors were resected from the two mice and fixed in 4% paraformaldehyde, processed routinely into paraffin, sectioned at 7 microns, stained H & E for 5 min. In order to detect the apoptotic or necrotic cells in tumor tissues, the rest section samples were stained with TUNEL. Images of these sections were taken using an upright digital microscope (DM 4000: Leica, Nussloch, Germany).

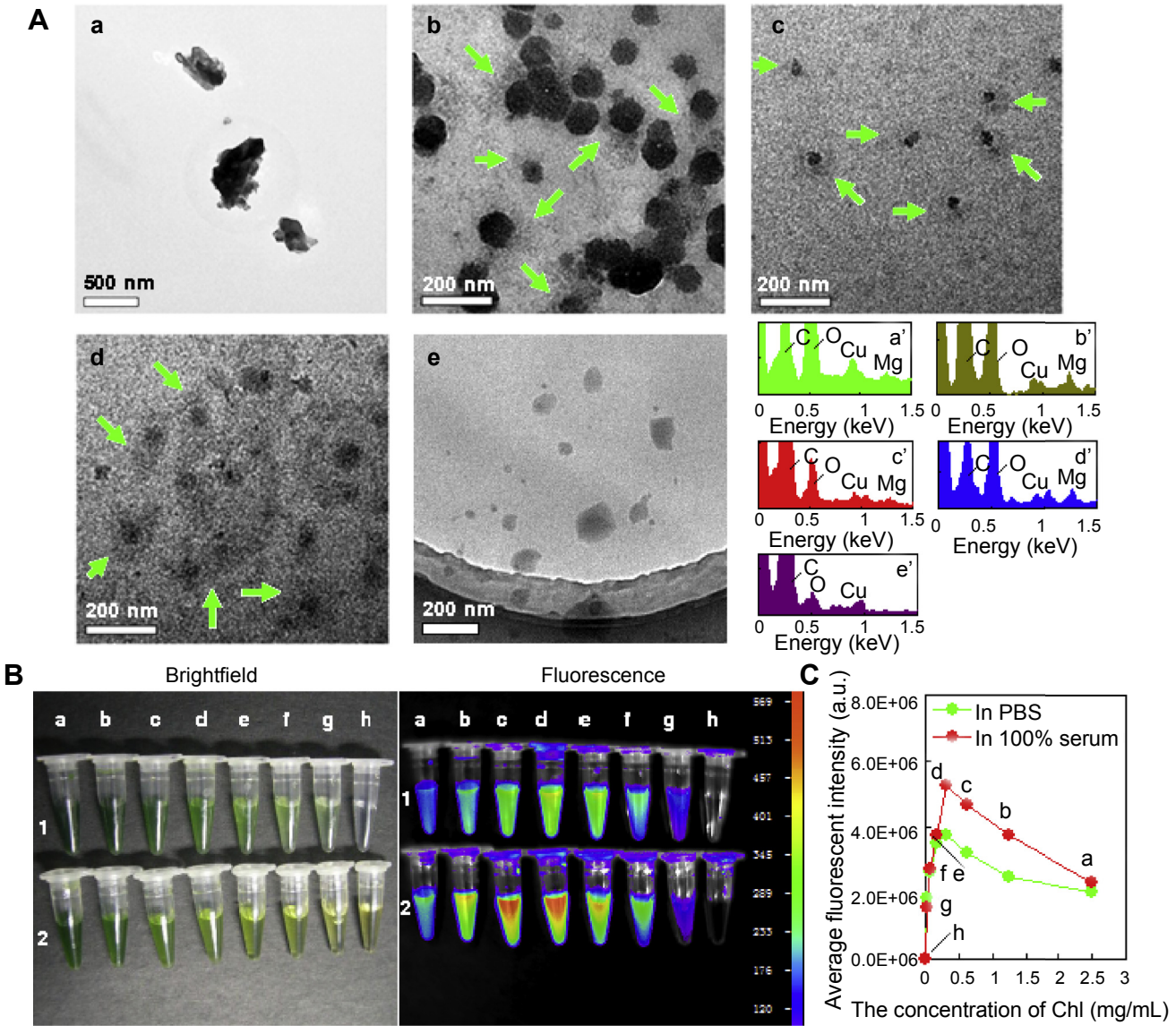

Fig. 3. Characterizations of the Plu–Chl nanocomposites. (A) HRTEM images and EDS spectra of (a, a') the pure Chl, (e, e') Plu and the Plu–Chl nanocomposites with the (b, b') 4:1, (c, c') 1:1 and (d, d') 1:4 mass ratios of Plu to Chl, respectively (some polymer shells were poined with the green arrows). (B) Brightfield image, and the corresponding fluorescence of the nanocomposites (Plu:Chl = 1:1) in PBS (row 1), and 100% serum (FBS, row 2). (C) The average fluorescence intensities at 700 nm for the Plu–Chl samples shown in the left hand images. The concentrations of Chl were 2.5 (column a), 1.25 (column b), 0.625 (column c), 0.313 (column d), 0.156 (column e), 0.078 (column f), 0.036 (column g), 0 mg/mL (column h (PBS or FBS)), respectively. (For interpretation of the references to color in this figure legend, the reader is referred to the web version of this article.)

2.2.13. Statistical analysis

The statistical significance was determined via an analysis of variance (ANOVA), followed by Tukey's post hoc test, and a P-value < 0.05 was considered as statistically significant; $P < 0.01$ was considered highly significant.

3. Results and discussion

3.1. Optical properties and morphology of the Plu–Chl nanocomposites

The fluorescent imaging showed that this plant leaves had bright NIR fluorescence, and the intensity of the fluorescence from the leaves was significantly higher than the intensity of that from the stems (Fig. 1). This suggested that the leaves were rich in Chl. Therefore we extracted Chl only from the leaves. The extracted Chl product was found to be in deep green color (in web version) with strong optical absorption between 600 and 700 nm (Supplementary Fig. 1). For enhanced dispersion, Chl is encapsulated in pluronic F68 polymer, to form a Plu–Chl nanocomposite as schematically illustrated in Fig. 2. Water solubility of the Plu–Chl nanocomposite was found to be much improved by the polymer encapsulation. For Chl suspended in water without Plu, however, deep green (in web version) precipitates formed rapidly. The ratio of Plu to Chl in the nanocomposite was optimized for water solubility and fluorescence intensity as shown in Supplementary Fig. 2. 1:1 ratio of Plu to Chl was used for the following cell and animal experiments.

Fig. 3A shows the HRTEM images and EDS spectra of water-insoluble Chl, Plu and Plu–Chl nanocomposites. As can be seen in Fig. 3A-a, pure Chl has an irregular geometry and dark contrast. The Plu particles shown in Fig. 3A-e are nearly spherical in shape with light gray color. The Plu–Chl nanocomposites appear to have dark cores of Chl and gray polymer shells of Plu. The sizes of the Chl particles are significantly reduced in the cores compared with the uncoated Chl (Fig. 3A, b–d). The average hydrodynamic sizes of those Plu–Chl nanocomposites are determined to be, respectively, 258.3 ± 171.2 nm (Plu:Chl = 1:4), 171.2 ± 85.13 nm (Plu:Chl = 1:1), and 191.8 ± 119.6 nm (Plu:Chl = 4:1) by PCS. Because each Chl molecule has one magnesium atom, the EDS spectra data show magnesium in Chl and Plu–Chl samples while that is not found in the Plu sample (Fig. 3A, a'e').

The Plu–Chl nanocomposites exhibit different fluorescent behaviors in varied medium such as PBS and serum. To compare their differences, the nanocomposites were dispersed in 100% FBS, in seven concentrations (from 0.036 to 2.5 mg/mL) of Chl. It was found that the Plu–Chl nanocomposites (Plu:Chl = 1:1) exhibit stronger NIR fluorescence when dispersed in FBS, compared to that of the same compound in PBS (Fig. 3B, C). This may have been because that the Chl was protected by the protein (FBS), and the Plu–Chl nanocomposites may have been better dispersed in FBS than in PBS, because of the steric hindrance that was produced between the nanocomposites by the long protein chains. The fluorescence intensity suffered slight loss when heated at 37 °C as the nanocomposites were dispersed in PBS. However, dispersion in FBS resulted in an intensity increase even after incubation for 144 h at 37 °C (Fig. 4). These interesting characteristics suggest advantageous of the Plu–Chl nanocomposites in long-term *in vivo* fluorescent imaging.

3.2. Uptake of Plu–Chl nanocomposites by cancer cells

Confocal fluorescent images show easy penetration of the cancer cells by the Plu–Chl nanocomposites. As shown in Fig. 5A, the melanoma cells (A375) emit bright red fluorescence after incubating of the cancer cells with the nanocomposites for only 0.5 h. The images along the horizontal section of the cells show that the fluorescent Plu–Chl nanocomposites have penetrated into the cytoplasm after only 0.5 h of incubation (Fig. 5B). Nearly no Plu–Chl nanocomposites have penetrated into nucleus, but these nanocomposites could stay in the cytoplasm for a long time, which were confirmed by the consecutive series of confocal slices (Fig. 5B and Supplementary Fig. 3). As can also be seen in Fig. 5A, the more nanocomposites migrate into cells after 6 h of incubation. Red fluorescence is seen to remain intensive in the cells even after more than two days (55 h), suggesting an ideal contrast agent for *in vivo* cancer imaging. It would also benefit cancer therapies because the

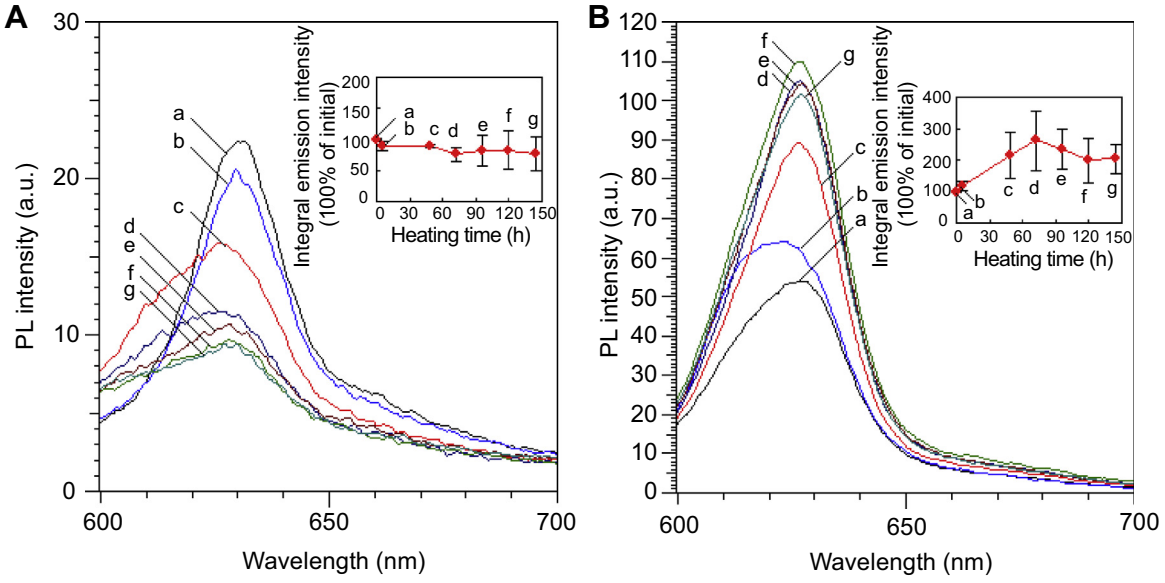

Fig. 4. The fluorescence stability of the Plu–Chl nanocomposites in (A) PBS, and (B) 100% serum (FBS), under heating at 37 °C for different times. Heating for (a) 0, (b) 5, (c) 48, (d) 72, (e) 96, (f) 120 and (g) 144 h. Insert: Average integrated emission intensity (% of initial) between 650 and 750 nm, for various heating time. The concentration of Chl was maintained at 0.05 mg/mL, and the mass ratio of Chl to Plu was maintained at 1:1. The excitation wavelength was 400 nm. Data shown in insert is expressed as mean ± standard deviation. Error bars were based on three simples per group.

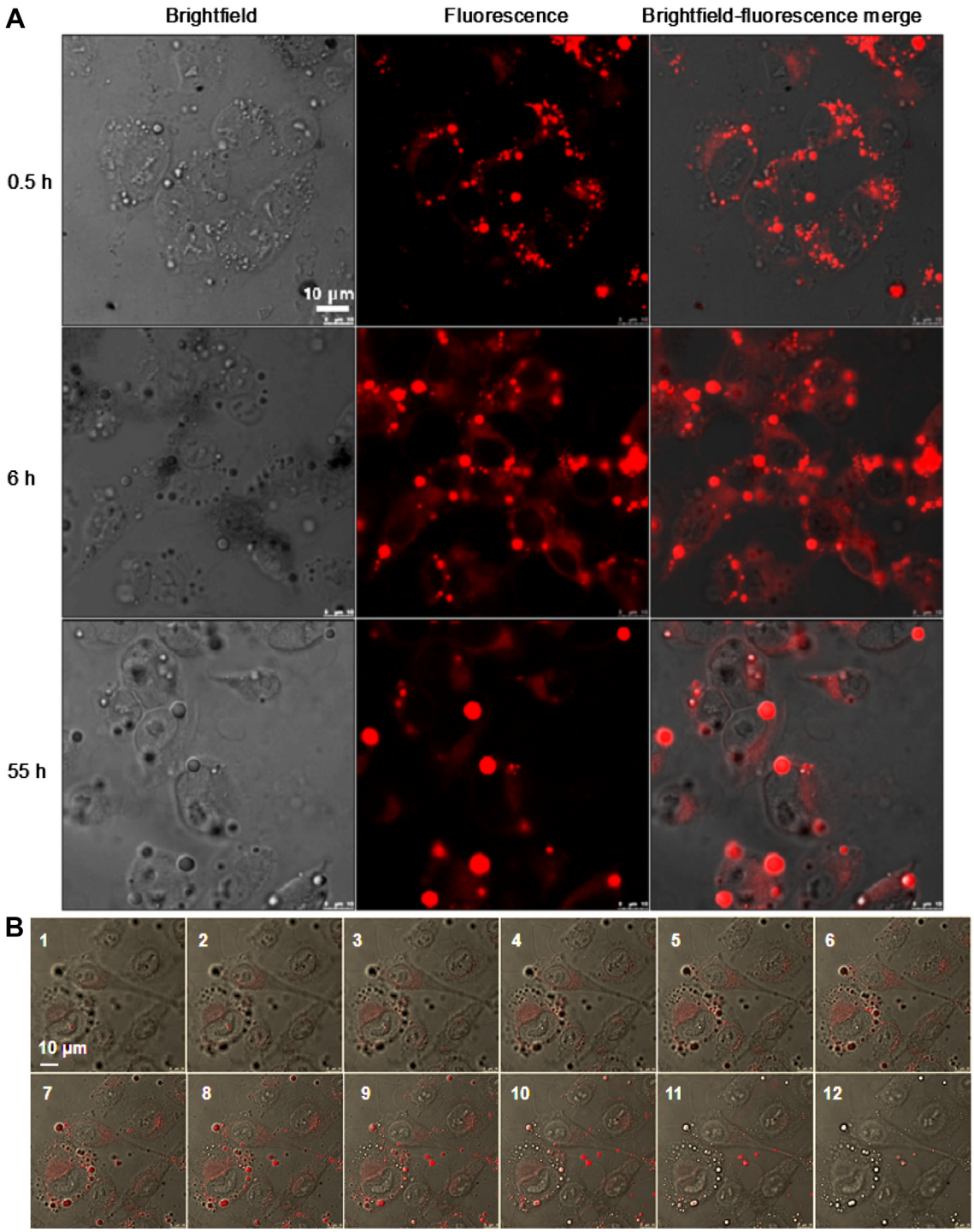

Fig. 5. Confocal fluorescence images of A375 cells incubated with Plu–Chl nanocomposites for different time. The concentration of Chl was 0.5 mg/mL, and the mass ratio of Plu to Chl in the nanocomposites was maintained at 1:1. Excitation filter: 488 nm; emission filter: 650–750 nm. Scale bar: 10 μm.

Chl could be used to kill cancer cells, via the long-term release of heat and ROS inside the cells under laser irradiation.

3.3. Plu–Chl nanocomposites passively targeting mouse tumors after tail vein injection

Passive tumor targeting of the Plu–Chl nanocomposites was investigated via tail vein injection. Fig. 6 shows the image of a nude mouse grown with melanoma (grown from A375 cells). As can be seen in this figure, weak autofluorescence is observed at the tumor site without Chl treatment. Only 2 min after tail vein injection of 200 μL of PBS-dispersed Plu–Chl nanocomposites (Chl = Plu = 10 mg/mL), the entire body of the melanoma-bearing mouse is seen to emit bright NIR fluorescence. In the initial 5 min after injection, the fluorescence intensity in the mouse upper body increases with time, which is the brightest part. This implied that the Plu–Chl nanocomposites might have migrated into the heart and lungs in a short time, following the blood circulation. In the period from approximately 30 min to 6 h after injection, the fluorescence gradually moves downwards to the middle part of the

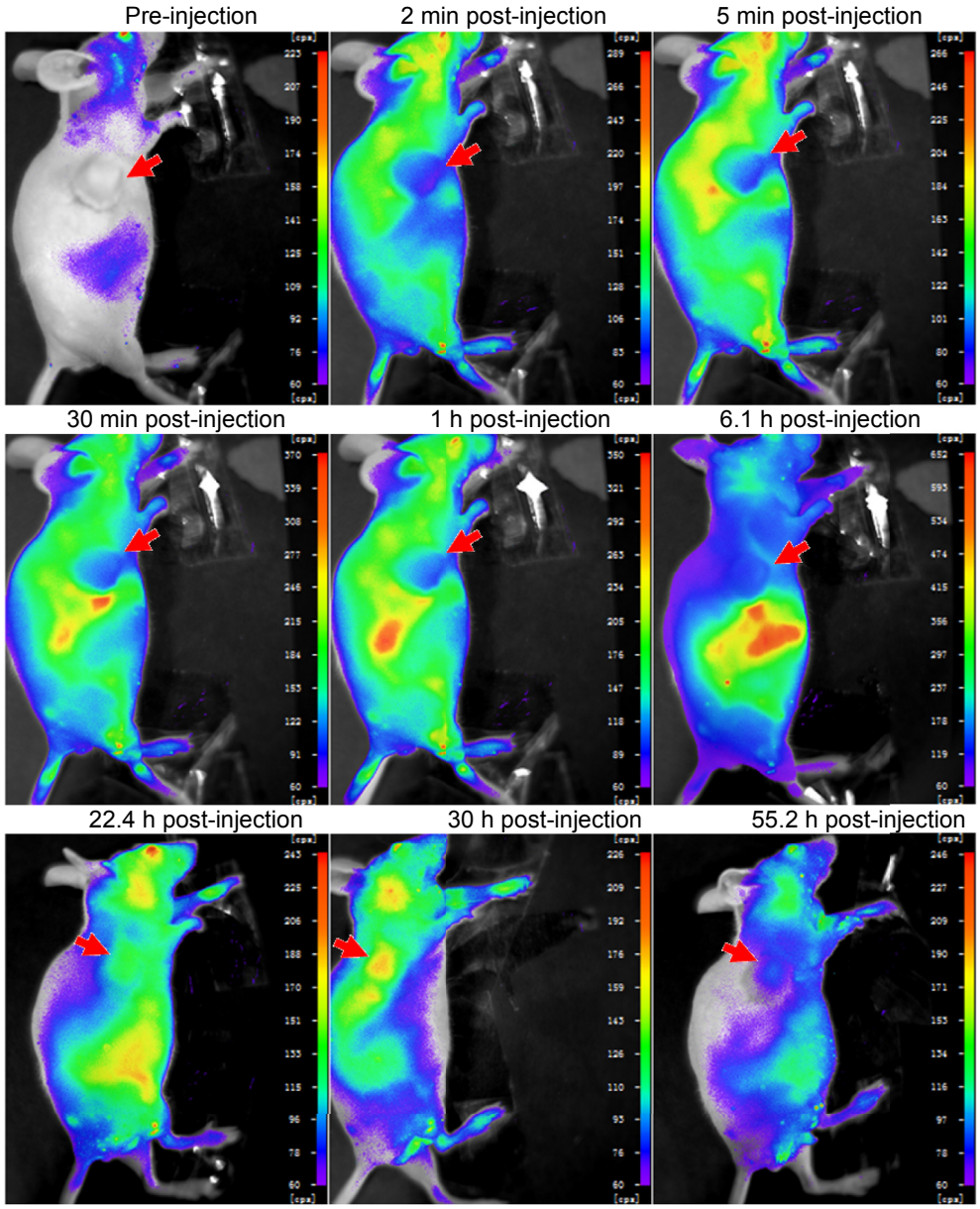

Fig. 6. Plu–Chl nanocomposites passively targeting the mouse melanoma tumor via tail vein injection, monitored using the *in vivo* imaging system. The tumor-bearing mice were injected with 200 μL of PBS-dispersed Plu–Chl nanocomposites (Chl = Plu = 10 mg/mL). The arrows point to the tumors.

body, which implied that the nanocomposites might have been uptaken mainly by the liver, spleen, and kidneys. The fluorescence intensity begins to decrease approximately 22 h after injection.

The fluorescence intensity at the tumor site was found to gradually increase during the initial 30 h, and reach the highest level at approximately 30 h post-injection. Although the flourescence begins to weaken in the following 24 h, it remains quite significant at the tumor site at 55 h post-injection (Fig. 6). These results indicate passively tumor-targeted Plu–Chl nanocomposites that are trapped by the tumor tissue for a prolonged time.

The *in vivo* imaging described above revealed the dynamic biodistribution of the Plu–Chl nanocomposites in the mouse body in real time. To directly observe the Chl fluorescence in mouse organs at certain time intervals after injection, other nude mice ($n = 9$) grown with melanomas were injected with PBS-dispersed Plu–Chl nanocomposite solutions (Chl = Plu = 10 mg/mL, 200 μL for each mouse) via their tail veins, and then sacrificed at 6, 30, and 55 h post-injection (three mice for each time), respectively. The hearts, livers, spleens, lungs, kidneys and tumors of the mice were resected and imaged using the *in vivo* imaging system. As a control, non-injected, tumor-bearing mice ($n = 3$) were sacrificed, and the organs and tumors were also resected and imaged. The results show no NIR fluorescence from the organs and tumors of the mice without injection of the Plu–Chl nanocomposites (Fig. 7A and Supplementary Fig. 4, row 1). In contrast, strong NIR fluorescence was observed at 6 h post-injection from the livers, spleens, lungs, kidneys, and tumors for the mice that were injected with the nanocomposites (Fig. 7A and Supplementary Fig. 4, row 2). The emission from hearts diminished for times longer than 6 h post-injection, while it remained in the tumors, kidneys, and other organs, which implied that most of the Plu–Chl nanocomposites had been cleaned from the blood and finally eliminated from the body through the kidneys. All mouse organs (except hearts) exhibited NIR fluorescence at 55 h post-injection, but the intensity was found

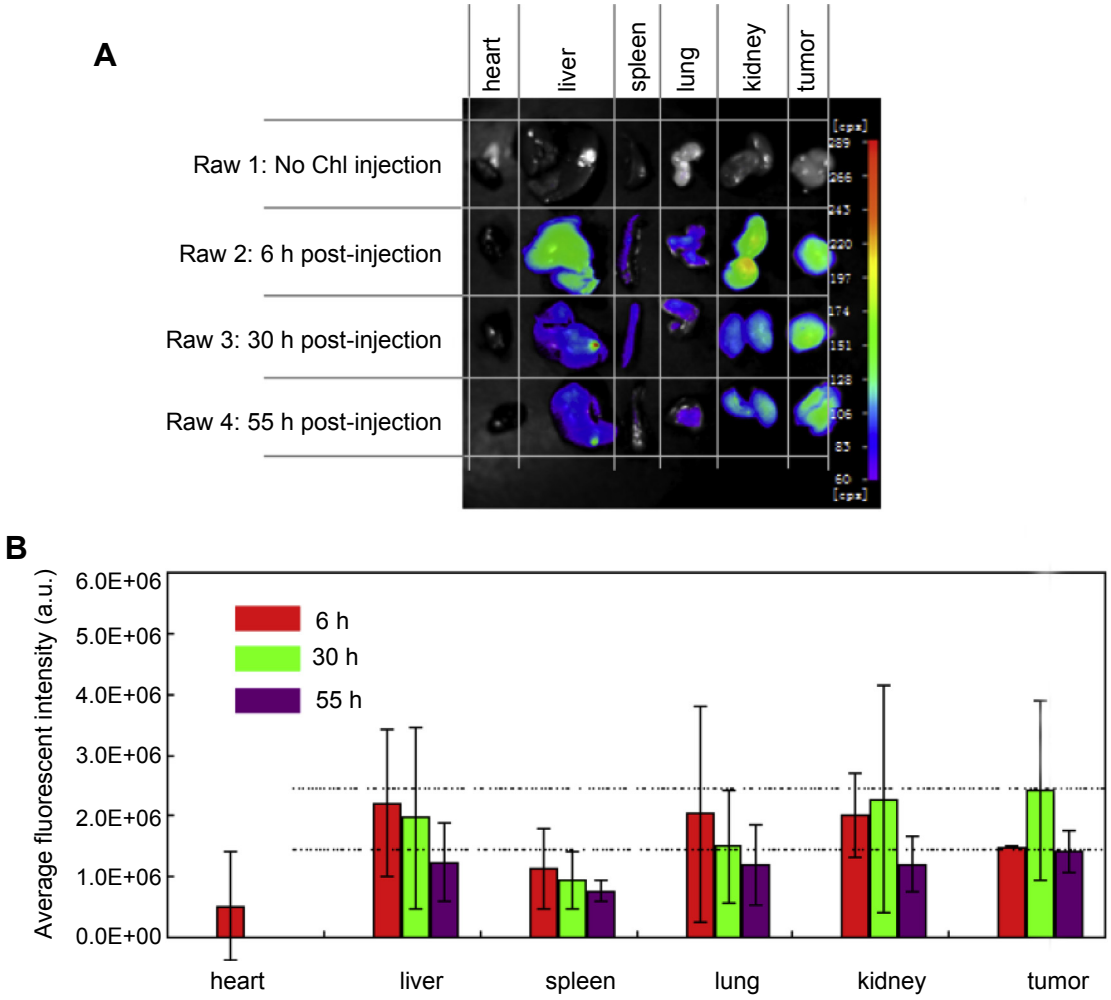

Fig. 7. Time-dependent biodistribution of Chl in the organs and tumors of the three groups of mice administered via tail vein injection and a control. (A) The fluorescent images of the organs and tumors resected from the mice and the control (The fluorescent images of the other mouse organs and tumors varying with time from the synchronized experiments are shown in Supplementary Fig. 4). (B) Semiquantitative biodistribution of Chl in the mice, analyzed via the averaged fluorescence intensity of each organ and tumor, using the software provided with the *in vivo* imaging system. The dotted lines are used to provide a convenient comparison between the fluorescence intensities of the tumors at 30 and 55 h post-injection and those of the other organs at 30 and 55 h post-injection. The tumor-bearing mice were injected with 200 μL of PBS-dispersed Plu–Chl nanocomposites (Chl = Plu = 10 mg/mL). Data was expressed as mean ± standard deviation. The error bars are based on the three groups of mouse organs and tumors shown in this figure (Fig. 7A) and Supplementary Fig. 4, and three mice per group.

to be lower than that at 30 h post-injection (Fig. 7A and Supplementary Fig. 4, rows 3 and 4). Note that the brightest fluorescence was observed in the tumors at 30 h post-injection (Fig. 7A and Supplementary Fig. 4, column f). This further demonstrates the effectiveness of the tumor-targed Plu–Chl nanocomposites via tail vein injection, without any antibody or peptide conjugation.

The semiquantitative fluorescence analysis shows decrease of the average NIR fluorescence intensity in livers, spleens, and lungs for times longer than 6 h post-injection, but those of the kidneys remain strong fluorescence until 30 h post-injection, and thereafter weaken at longer times (Fig. 7B). This further confirmed that after being injected through the tail veins, the Plu–Chl nanocomposites may be excreted from the mice via urination. Interestingly, the tumor fluorescence significantly increased in the first 30 h post-injection. At 30 h post-injection, the tumor fluorescence intensity was higher than those of other organs (Fig. 7B, see upper dashed line). In addition, although the average fluorescence intensity of the tumors at 55 h decreased to a level similar to that at 6 h post-injection, the intensity at this time point (55 h) was still higher than that of the other organs (Fig. 7B, see bottom dashed line). These kinetics data from tumor targeting are consistent with *in vivo* imaging results described above.

3.4. Plu–Chl nanocomposites passively targeting mouse tumors after gavage

It was found that mouse tumor targeting is also possible by having the Plu–Chl nanocomposites administered orally. In this work, the tumor-bearing mice were fed with PBS-dispersed Plu–Chl nanocomposites (Plu = Chl = 10 mg/mL, 0.5 mL for each mouse) by intragastric administration. The biodistribution and clearance of Chl in the mouse body were monitored in real time, using the *in vivo* fluorescence imaging technique. The results showed rapidly diffused NIR fluorescence throughout the entire mouse abdomen, including the bladder and tumor, within approximately 0.5 h post-gavage. Its NIR fluorescence intensity at the tumor site retained at high levels even at more than 72 h post-gavage (Fig. 8 and Supplementary Fig. 5).

Upon sacrificing the mice ($n = 15$) and resecting the organs and tumors at different times (using three mice for each time) after

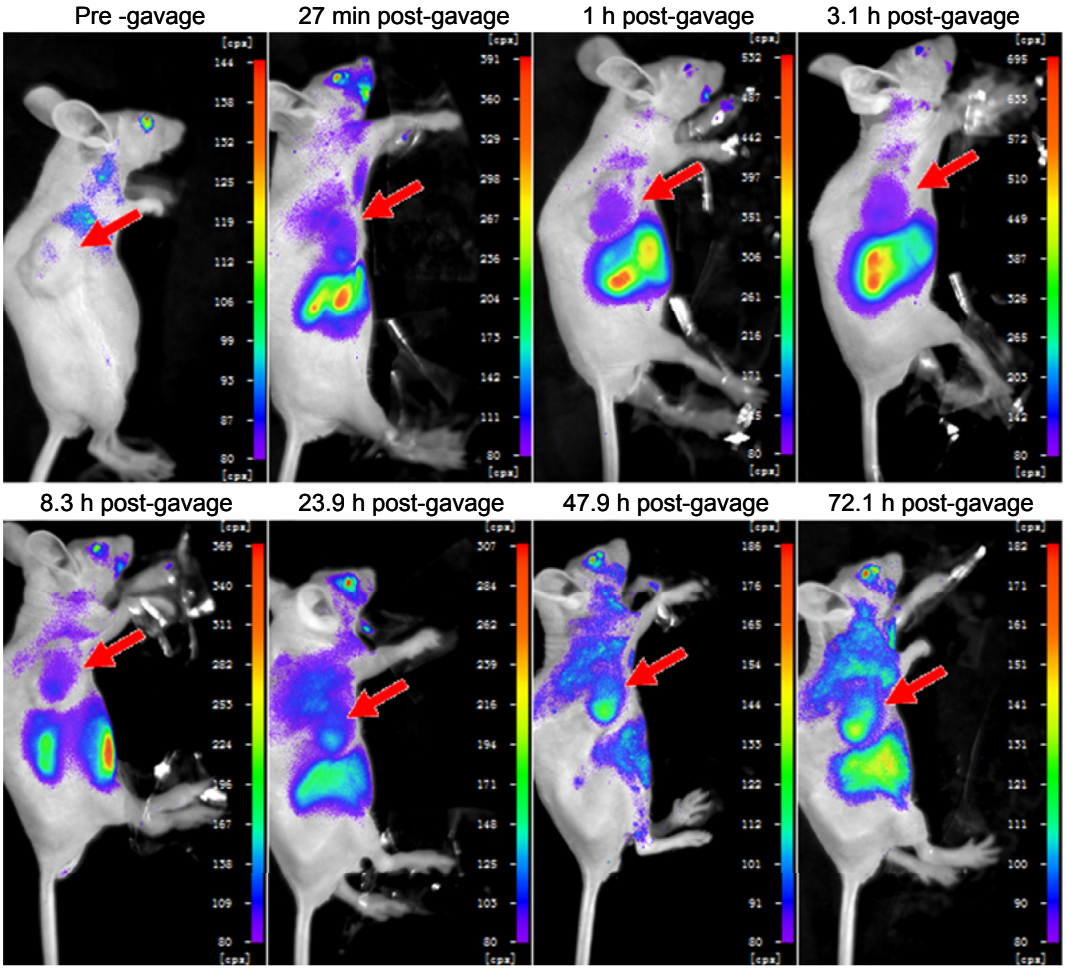

Fig. 8. Plu–Chl nanocomposites passively targeting the mouse melanoma tumor via intragastric administration, monitored (recumbent position) using the *in vivo* imaging system. A fluorescence image of this mouse in the supine position is shown in Supplementary Fig. 5). The tumor-bearing mouse was administered with 0.5 mL of PBS-dispersed Plu–Chl nanocomposites (Chl = Plu = 10 mg/mL). The arrows point to the tumors.

intragastric administration, the fluorescent images showed bright fluorescence from the tumor at 3, 8, 24, and 72 h post-gavage (Fig. 9A and Supplementary Fig. 6). The average fluorescence intensities of the tumors and other organs including livers, spleens, lungs, and kidneys all increased during the initial 8 h post-gavage, and then subsequently decreased over time (Fig. 9B). However, the tumor fluoresce intensities at 8, 24, and 72 h post-gavage were always higher than those of other organs at the same time points (Fig. 9B, see dashed lines). At 168 h post-gavage, no NIR fluorescence was observed from the tumors and organs of the mice, similar to the mice that were not fed with any Chl. These results indicate effective passive tumor-targeting of the Plu–Chl nanocomposites that are well retained within the tumor sites for at least three days (but less than six days) when administered intragastrically.

Oral administration of the Plu–Chl nanocomposites can be a safe and convenient route. It can also alleviate the suffering of patients compared to other approaches such as injection. The oral administration mode in real-time cancer imaging may also have considerable clinical advantages over intravenous injection.

It should be noted that the liver, spleen and lung also emit bright fluorescence, this is because that macrophages are diffusely scattered in these organs. It is known that solid tumor tissues typically lack of effective lymphatic drainage and contain large numbers of blood vessels to feed their growing demand for nutrients. They tend to form vessels that are abnormal in form and architecture (leaky vasculatures). Nanoparticles such as silicon [18] accumulate in tumors much more readily than they do in normal tissues, due to enhanced permeability and retention (EPR) effect. In this work, the passive tumor targeting effect of Plu–Chl nanocomposites is mainly due to EPR.

3.5. Photothermal conversion of the Plu–Chl nanocomposites upon laser irradiation

It was found that Chl converted NIR laser light into heat with high efficiency. This interesting finding suggested that the Plu–Chl nanocomposites could not only be used for *in vivo* cancer target imaging, but also for cancer PTT. We selected a laser with a wavelength of 671-nm to induce the photothermal conversion and phototherapy of the Chl. The reasons are as follows: Chl has a maximum absorption peak around 671-nm; melanoma is suitable for phototherapy since this tumor usually locates under skin surface; many reports have been demonstrated that the laser light with 600–700 nm wavelength range could be successfully used for melanoma phototherapy both in clinic and animal experiments [19-22]. For temperature measurement, the initial temperature of the solutions was maintained at 25.1 ± 0.1 °C. A Plu–Chl solution (Plu = Chl = 8 mg) was dropped on a Parafilm, dried naturally, and then irradiated by laser. A damaged region was identified in the film

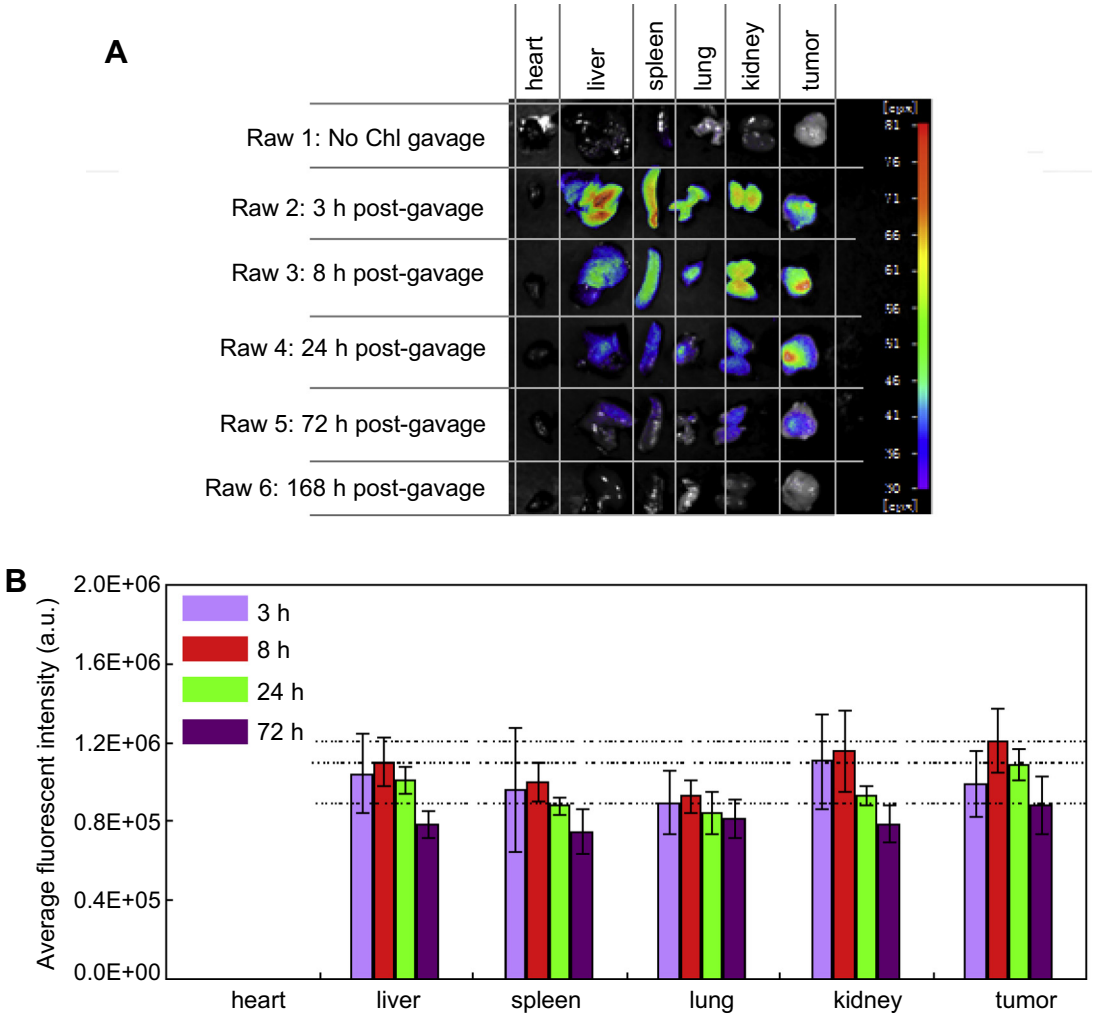

Fig. 9. Time-dependent biodistribution of Chl in the organs and tumors of the three groups of mice administered via intragastric administration and a control. (A) The fluorescent images of the organs and tumors resected from the mice and the control (The fluorescent images of the other mouse organs and tumors varying with time from the synchronized experiments are shown in Supplementary Fig. 6). (B) Semiquantitative biodistribution of Chl in the mice, analyzed via the averaged fluorescence intensity of each organ and tumor, using the software provided with the *in vivo* imaging system. The dotted lines provide a convenient comparison between the fluorescence intensities of the tumors at 8, 24, and 72 h post-gavage and those of the other organs, also at 8, 24 and 72 h post-gavage. The tumor-bearing mouse was administered with 0.5 mL of PBS-dispersed Plu–Chl nanocomposites (Chl = Plu = 10 mg/mL). Data was expressed as mean ± standard deviation. The error bars were based on the three groups of mouse organs and tumors shown in this figure (Fig. 9A) and Supplementary Fig. 6, and three mice per group.

only after ~30–40 s irradiation. In contrast, the Parafilm covered with Plu alone remained intact after irradiation (Fig. 10A–B).

As shown in Fig. 10C, the temperature of the 200 μL Plu–Chl nanocomposite aqueous solution containing only 0.5 mg/mL of Chl increases to above 23 °C after 5 min of irradiation; and over 30 °C after 20 min of irradiation, indicating a rapid temperature increase initially. Reducing the Chl concentration to 0.25 and 0.1 mg/mL resulted in the solution temperature increase at lower rates, to over 24 °C and 20 °C after 20 min of irradiation, respectively. However, for even higher Chl concentration of 5 mg/mL, laser light was not able completely penetrate the solution. In this case, the portion of the Chl molecules that is not exposed to laser does not participate in heat generation. As consequence, the temperature increase rate of the 5 mg/mL Plu–Chl sample was only slightly higher than that of the 0.5 mg/mL sample, especially at the first couple of minutes. In a control experiment, the temperature of a 200 μL aqueous solution containing only Plu (1 mg/mL) increased by less than 6.8 °C after 20 min of irradiation, close to the temperature increase in a PBS solution (about 6.1 °C).

3.6. Intracellular ROS generated by Plu–Chl nanocomposites after laser irradiation

3.6.1. Qualitative analysis of the ROS

Using Chl for cancer phototherapy is expected to be highly efficient, for its capability in generating ROS for PDT after 671-nm laser irradiation (Fig. 11). The efficiency of PTT of Chl can be well improved by PDT. In this experiment, DCFH-DA was used to detect intracelluar ROS, whose level is determined by fluorescence intensity (at 525 nm), generated by the reaction product (DCF) of ROS and DCFH. Chl exhibits strong fluorescence from 650 nm to 750 nm, but weak intensity between 500 nm and 540 nm. Therefore, the fluorescence of Chl has a negligible influence on the ROS measurements. As shown in Fig. 11A, when the melanoma cells (A375) were incubated with the culture medium (RPMI 1640, without serum)-dispersed Plu–Chl nanocomposites containing 0.5 mg/mL of Chl, and then irradiated with the 671-nm laser for 20 min, the confocal fluorescent image showed that most of the cells emitted green fluorescence. In the absence of irradiation, however, the

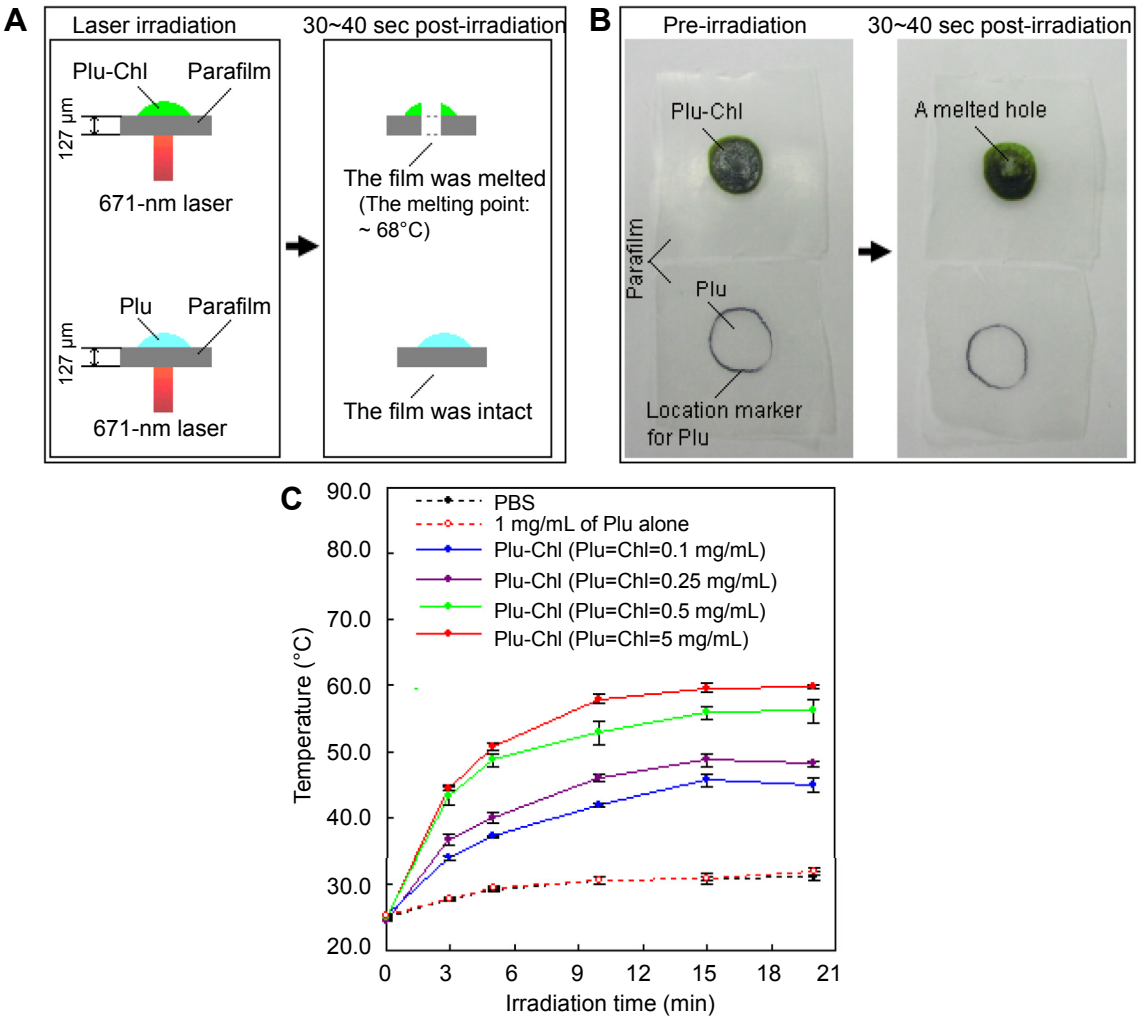

Fig. 10. Photothermal effect of Chl induced by 671-nm laser irradiation and controls. (A) Schematic diagram and (B) experiment of a Parafilm (thickness: 127 μm) covered with dry Plu–Chl and Plu before and after irradiation; (C) Temperature increase in the 200 μL of Plu–Chl nanocomposite, PBS and Plu solutions after irradiation. Data was expressed as mean ± standard deviation. Error bars were based on three times per time point.

cells incubated with the Plu–Chl nanocomposites exhibited practically no fluorescence. This was observable and direct evidence that showed that the laser irradiation at 671-nm was extremely effective in inducing the Plu–Chl nanocomposites to generate intracellular ROS.

3.6.2. *Quantitative analysis of the ROS*

A SpectraMax M5 Universal Microplate Spectrophotometer (Molecular Devices Inc., Sunnyvale, CA, USA) was used to measure the fluorescence intensity (at 525 nm) of the cells treated with the nanocomposites and irradiation. A375 cells were incubated with two Plu–Chl nanocomposites containing 0.1 and 0.5 mg/mL of Chl, respectively, and irradiated with laser for 20 min (Fig. 11B). The intracellular ROS levels are 29.33 ± 11.01 and 51.60 ± 13.68 times higher than that of the control sample (untreated cells). In absence of irradiation, the intracellular ROS levels are only 1.62 ± 0.54 (the sample containing 0.1 mg/mL of Chl) and 1.60 ± 0.50 (the sample containing 0.5 mg/mL of Chl) times higher than that of the control. These levels are close to those measured for irradiation on cells alone for 20 min (1.09 ± 0.17 times higher than in the control). In addition, Plu alone generated almost no ROS, with or without irradiation. The results presented above indicated that it was only Chl in the culture medium-dispersed Plu–Chl nanocomposites that generated high levels of intracelluar ROS after irradiation.

It is known that ROS can induce cellular toxicity and tissue damage in cancer PDT, which is being tested for clinical use in oncology [23]. PDT is usually combined with hyperthermial treatments, to enhance the efficacy of cancer treatment. For such bifunctional materials, some hyperthermial reagents (*e.g.*, carbon-based nanomaterials [24,25] and gold nanostructures [26–28]) have been incorporated into photosensitizers. In this work, however, the Chl already possessed photothermal and photodynamic properties, so they did not have to be combined with other photosensitizer materials. This is a unique advantage of Chl for much more efficient medical theranostics.

3.7. *In vitro phototherapy effect of the Plu–Chl nanocomposites*

3.7.1. *Qualitative analysis of cell viability*

Nearly all A375 cells disintegrated or became crimpled after incubated with Plu–Chl nanocomposites containing only 0.5 mg/mL of Chl, and irradiated with the 671-nm laser for 20 min (Fig. 12A, left). In contrast, cells appeared to be not affected when incubated with the nanocomposites, but without NIR irradiation (Fig. 12B, left). If only incubated with Chl but no Plu, the cell state after

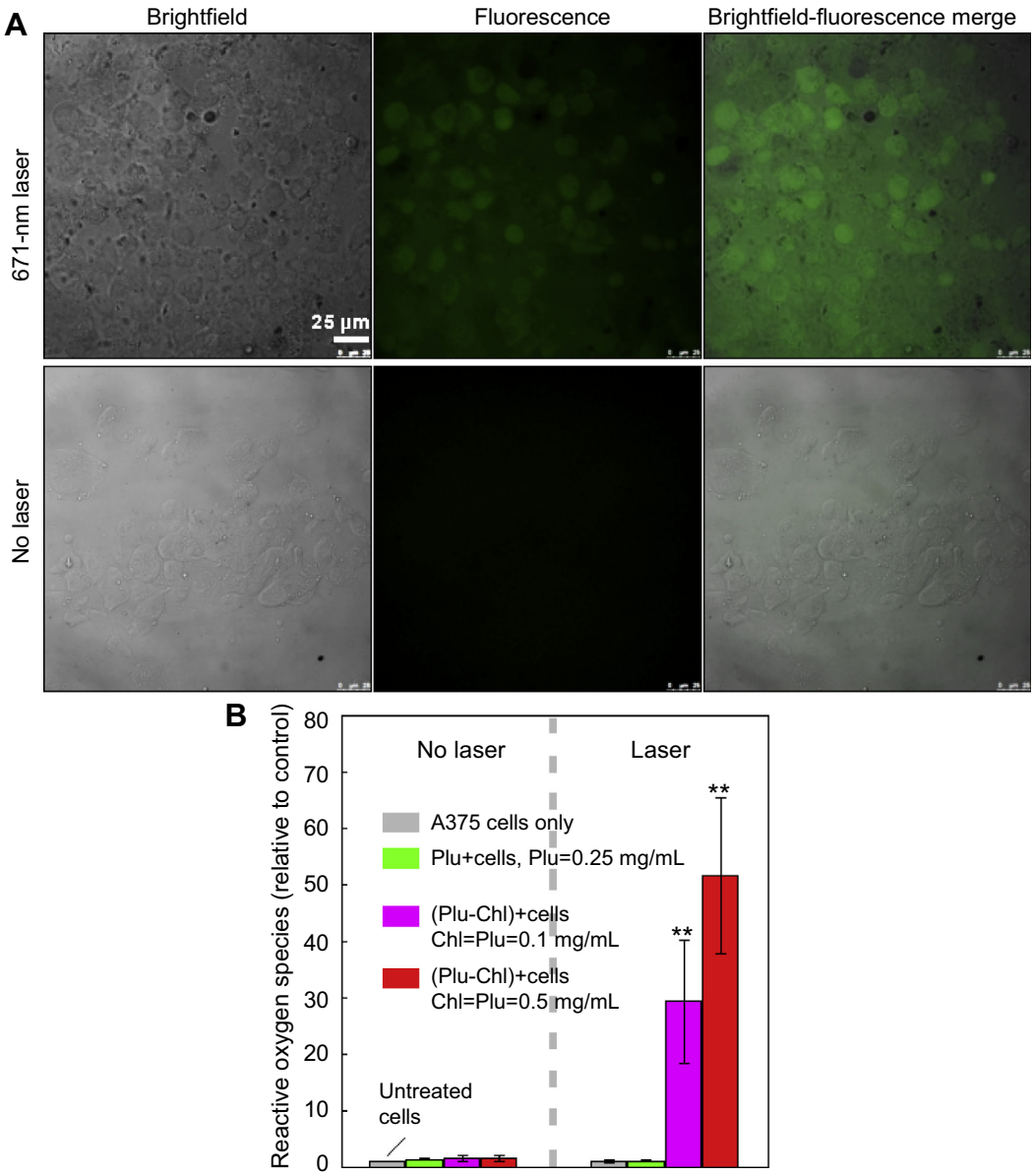

Fig. 11. ROS produced by the Plu–Chl nanocomposites in A375 cells, without and with 20 min of 671-nm laser irradiation. (A) Confocal images. The concentration of Chl was 0.5 mg/mL. Excitation filter: 488 nm, emission filter: 500–540 nm. Scale bar: 25 μm. (B) ROS levels in the A375 cells generated by Plu–Chl nanocomposites containing different concentrations of Chl, and controls. The significance level observed was ** $P < 0.01$, in comparison with the group values of cells alone after 20 min of laser irradiation. Data was expressed as mean ± standard deviation. Error bars were based on five simples per group.

irradiation was close to that observed for cells incubated only with the culture medium (with or without irradiation) (Fig. 12A, middle and right; Fig. 12B, right). These are experimental evidences that the laser alone had no effect on the cell growth, and the Plu played an important role in cell-killing efficiency of Chl. For the cells incubated with the well-dispersed Plu–Chl nanocomposites, nearly all of the cancer cells emitted red fluorescence (Fig. 12, left), which implied that the Chl might only significantly penetrate into the cancer cells—and subsequently kill them under irradiation—when it was dispersed by the Plu.

3.7.2. Quantitative assay of cell viability

Effective laser-induced cell killing by the Plu–Chl nanocomposites was further demonstrated in a cell viability quantification assay. As shown in Fig. 12C, when the A375 cells were incubated with nanocomposites containing 0.05, 0.15, and 0.5 mg/mL of Chl, and irradiated for 20 min using the 671-nm laser, the cell viabilities were 85.72 ± 4.85, 30.48 ± 6.43, and 0.36 ± 0.44%, respectively. As a control, the cells were incubated with the same nanocomposite in the absence of irradiation. In this case, the cell viabilities were close to 100% (from 94.26 ± 9.1 to 101.68 ± 12.71%). If the cells were incubated with 0.5 mg/mL of Chl with no Plu, the cell viabilities were 95.64 ± 4.09% (with irradiation) and 99.75 ± 10.44% (without irradiation), respectively.

3.8. In vivo phototherapy effect

Although the Plu–Chl nanocomposites could passively target mouse tumors after tail vein injection or gavage, the concentration of Chl trapped by the tumors was not high enough to efficiently inhibit tumor growth after laser irradiation (Supplementary Figs. 7 and 8). Intratumoral injection was therefore used for the

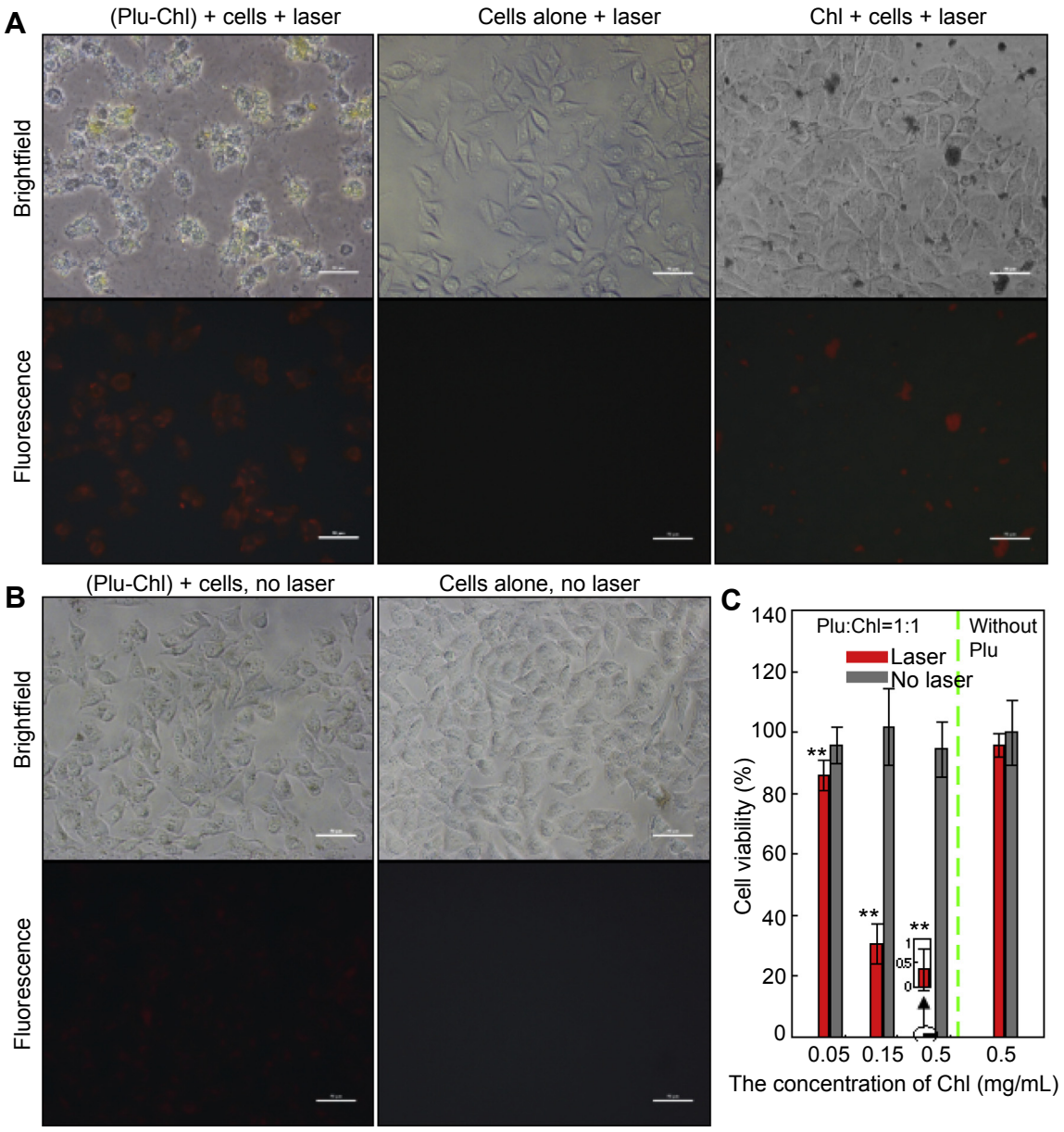

Fig. 12. Brightfield and corresponding fluorescence images, and cell viabilities of A375 cells after incubation with Plu–Chl nanocomposites, under 671-nm laser irradiation, and controls. (A) Laser. (B) No laser. The concentration of Chl in all samples was maintained at 0.5 mg/mL. Scale bar: 50 μm. (C) The viability of A375 cells incubated with Chl or Plu–Chl nanocomposites with and without irradiation. The significance level observed was * *$P < 0.01$, in comparison with the no irradiation groups. Data was expressed as mean ± standard deviation. Error bars were based on five simples per group.

phototherapy performed in this work. Local treatment is a popular cancer phototherapy method using nanomaterials [17,24,28]. This method ensures that tumors contain high concentrations of heat reagents for a long time, and the heat generated by the locally injected materials can specifically destroy tumors.

Some Plu–Chl nanocomposites were found retain in mouse tumor for at least seven days after intratumoral injection (Fig. 13 A). However, many of the Chl molecules may diffuse into body rapidly since the fluorescent intensity in tumor obviously decreased in 3 days after injection (Fig. 13 B). As shown in Fig. 13 (C and D) and Supplementary Fig. 9, the analysis of the semiquantitative biodistribution of Chl in the mice over time suggested that some Chl molecules migrated into livers 5 h after intratumoral injection. The spleens, lungs and kidneys also contained a few Chl. Many Chl may be cleaned by mice 27 h after injection. Therefore, to improve phototherapeutic efficiency, Plu–Chl nanocomposites containing 5 mg/mL of Chl (70 μL for each mouse and each time) were injected into the tumors every three days for three times, in order to maintain a high Chl concentration in the tumors. The results showed clear growth inhibition of all mouse melanoma tumors ($n = 5$) that were injected with the nanocomposites after 15 days of irradiation (Fig. 14A(left), Fig. 14D (red line) and Supplementary Fig. 10A). In contrast, the mouse tumors grew markedly over time when injected with the same amount of nanocomposites but without irradiation ($n = 5$) (Fig. 14A (right), Fig. 14D (black line) and Supplementary Fig. 10B), or injected with Plu alone with irradiation ($n = 4$) (Fig. 14B, D (pink line in web version) and Supplementary Fig. 11). This is similar to the tumors that did not subject to injection or irradiation (Fig. 14C, D (green line) and Supplementary Fig. 12). Compared with the tumors treated with the Plu–Chl

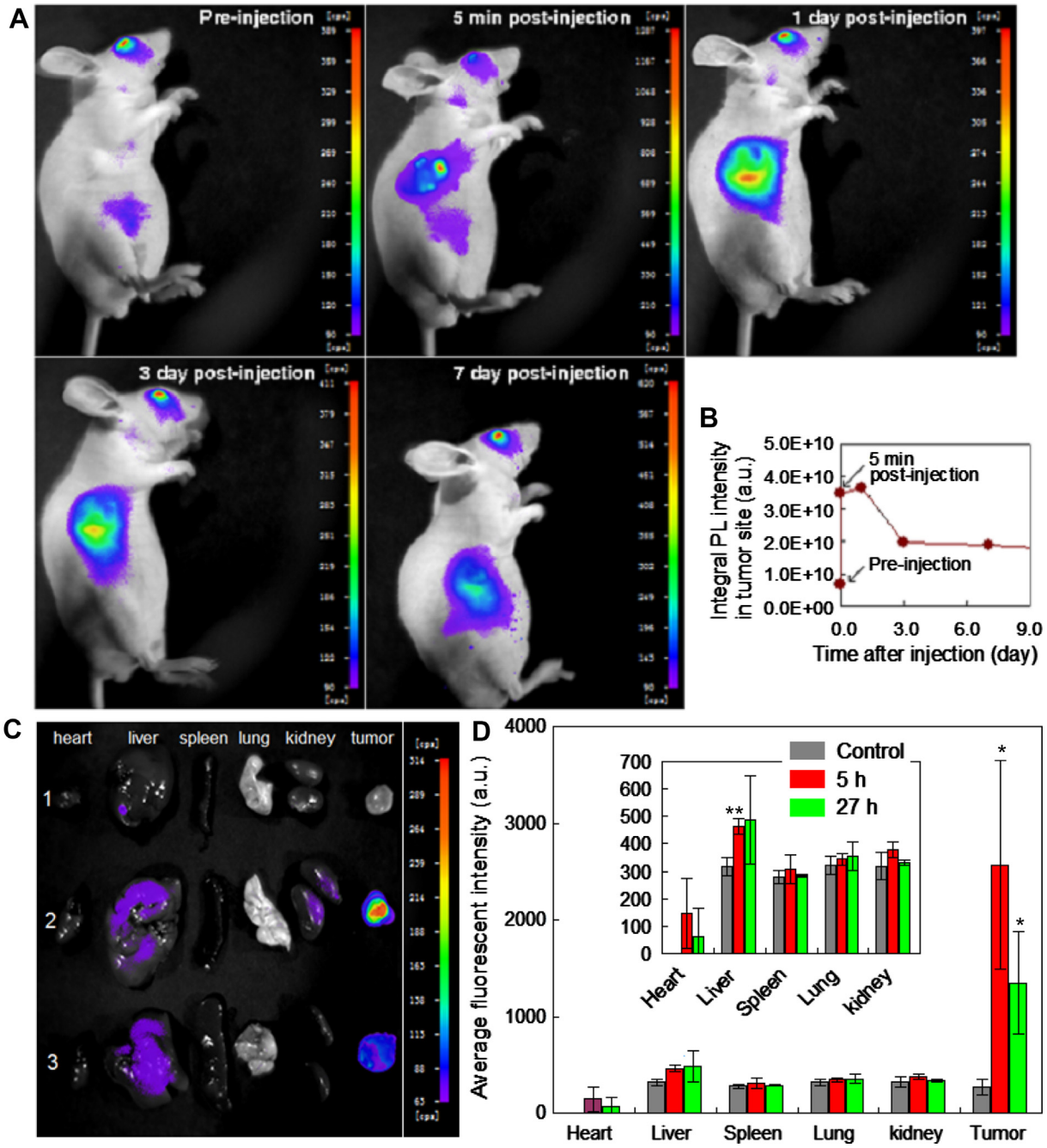

Fig. 13. The retention of the Plu–Chl nanocomposites at the tumor site. (A) *In vivo* fluorescence imaging over time after injection. (B) Integral photoluminescence (PL) intensity at the tumor site varying over time based on the mouse shown in (A). (C) The Plu–Chl nanocomposites redistributed in the mouse tumors and main organs over time after injection (The fluorescent images of the other mouse organs and tumors varying with time from the synchronized experiments are shown in Supplementary Fig. 9). The organs and tumors were resected from the mice without Chl treatment (row 1), and at 5 (row 2) and 27 h (row 3) post-injection with Plu–Chl nanocomposites. (D) Semiquantitative biodistribution of Chl in the mice over time after injection, analyzed via the averaged fluorescence intensity of each organ and tumor, using the software provided with the *in vivo* imaging system. The tumor-bearing mice were intratumorally injected with 70 μL of PBS-dispersed Plu–Chl nanocomposites (Chl = Plu = 5 mg/mL) and PBS-dispersed Plu (5 mg/mL). The significance level observed was * $P < 0.05$ and * *$P < 0.01$, in comparison with the control group (without Chl injection). Data was expressed as mean ± standard deviation. The error bars are based on the three groups of mouse tumors and organs shown in this figure (Fig. 13C) and Supplementary Fig.9, and three mice per group.

nanocomposites and laser irradiation, the surfaces of the tumors in all control groups were not damaged.

When the tumor-bearing mice were intratumorally injected with PBS-dissolved Plu aqueous solution, this aqueous solution would diffuse from the tumors quickly. These tumors may be similar with those without injection or may contain only small amount of Plu. Therefore, the result of the mouse tumors being injected with PBS-dissolved Plu alone with irradiation may be similar with that of laser irradiation alone, since the temperature increase of the PBS-dissolved Plu aqueous solution after 20 min of irradiation was very low (Fig. 10C).

To investigate the tumor tissue after laser irradiation, two tumor-bearing mice were intratumorally injected with the nanocomposites. In the case of tumor irradiated over a 3-day period (irradiated for 20 min every 24 h), the H & E staining results showed discontinuous tissue structure, significant size reduction,

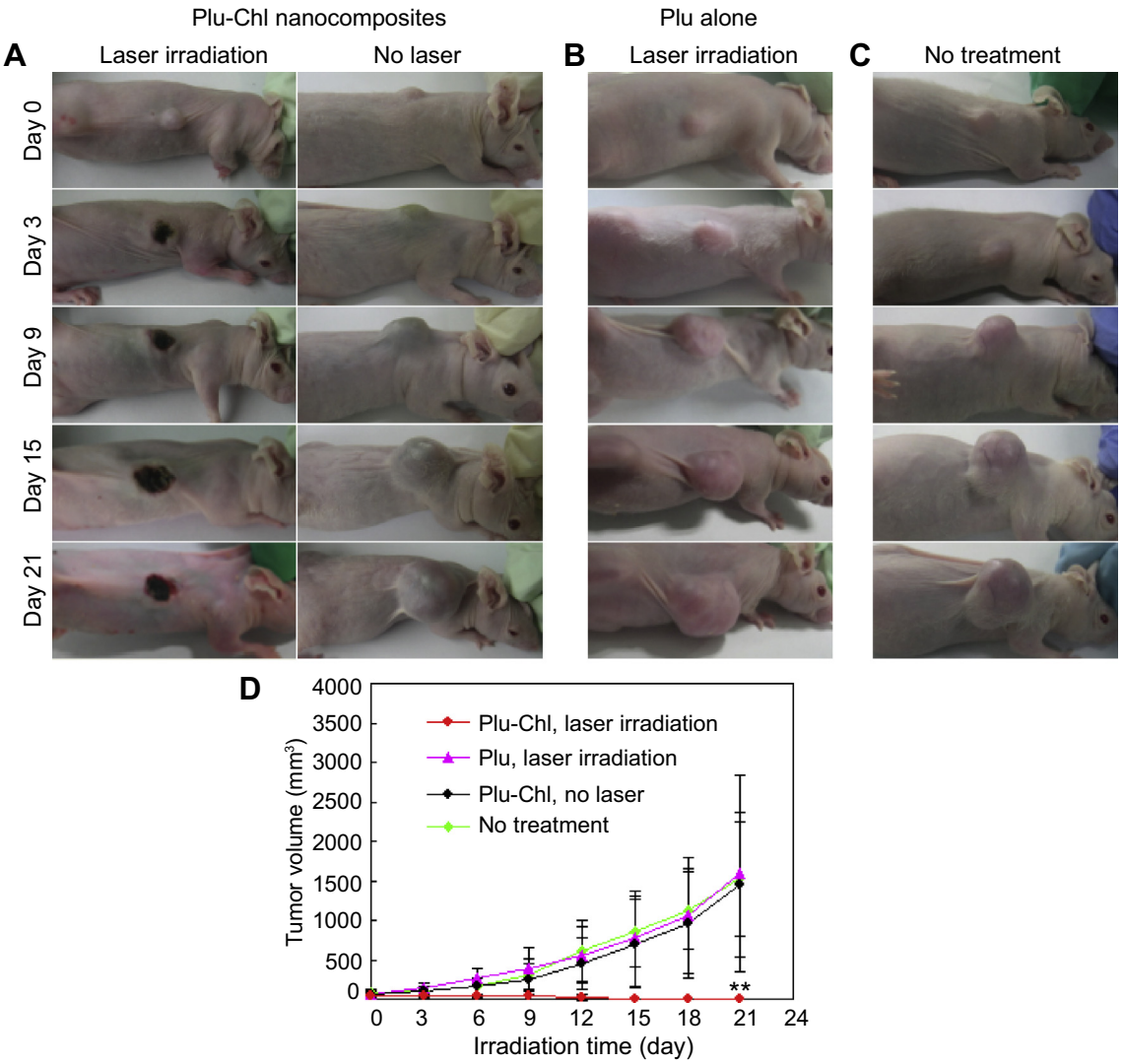

Fig. 14. *In vivo* phototherapy with intratumorally injected Plu–Chl nanocomposites under irradiation, and controls. Representative photographs of mice (A) intratumorally injected with PBS-dispersed Plu–Chl nanocomposites with (left), and without (right) 671-nm laser irradiation, and (B) intratumorally injected with PBS-dispersed Plu with 671-nm laser irradiation, and (C) without treatment. Photographs of the tumors in all mice are shown for various irradiation times in Supplementary Figs. 10–12. (D) Growth curves of tumors in the mice, based on the mice shown in this figure and Supplementary Figs. 10–12. Data was expressed as mean ± standard deviation. Error bars were based on five or four mice per group.

and some cells disintegration (Fig. 15A(left)). In addition, the tumor blood vessels were either significantly reduced or severely damaged. Whereas, for the non-irradiated tumor, H & E staining images showed undamaged blood vessels, evenly distributed tumor cells, and well-organized cell structures (Fig. 15A(right)).

The tumor tissue damage was also examined using the TUNEL assay. As shown in Fig. 15B(left), many cancer cells in tumor tissue exhibited brown color (in web version) which indicated that these cells died after treatement with the Plu–Chl and laser irradiation since only necrotic or apoptotic cells were stained brown. In addition, there are clearly morphological changes in this tumor tissue. For example, the cells were shrunken and arranged loosely. As a control, however, the cancer cells were stained with blue color (Fig. 15B(right)), which indicated that these cells were not affected since the robust and viable cells were stained blue. In this control group, it can be seen that the cancer cells were arranged tightly and the cytoplasms and necleis were full (Fig. 15B(right)). These results further demonstrate the therapeutic effectiveness of the Plu–Chl nanocomposites in a short time by laser irradiation.

4. Conclusions

We have discovered that the dietary Chl encapsulated with Plu polymer nanoprticles could be used for cancer imaging after vein injection or oral administration. Although cancer target imaging via both intravenous injection and oral administration of the Plu–Chl nanocomposites would be beneficial for time-consuming clinical surgery, oral administration is convenient compared to the intravenous injection. As evidenced in the experimental results, the photothermal effect of Chl is another major discovery of this research, that is successfully applied in cancer treatment in vitro and *in vivo* with high efficiency. This therapy was highly efficient because Chl exhibited both photothermal and photodynamic properties. The mouse melanoma tumors are eliminated after 15 days of irradiation via intratumorally injected nanocomposites. The tumor tissues are also seriously damaged only after 3 days of irradiation. Since the bio-safety of Chl is well established as a natural material and an important component in our daily diet, the results presented by this work may be highly attractive for doctors and patients in the future.

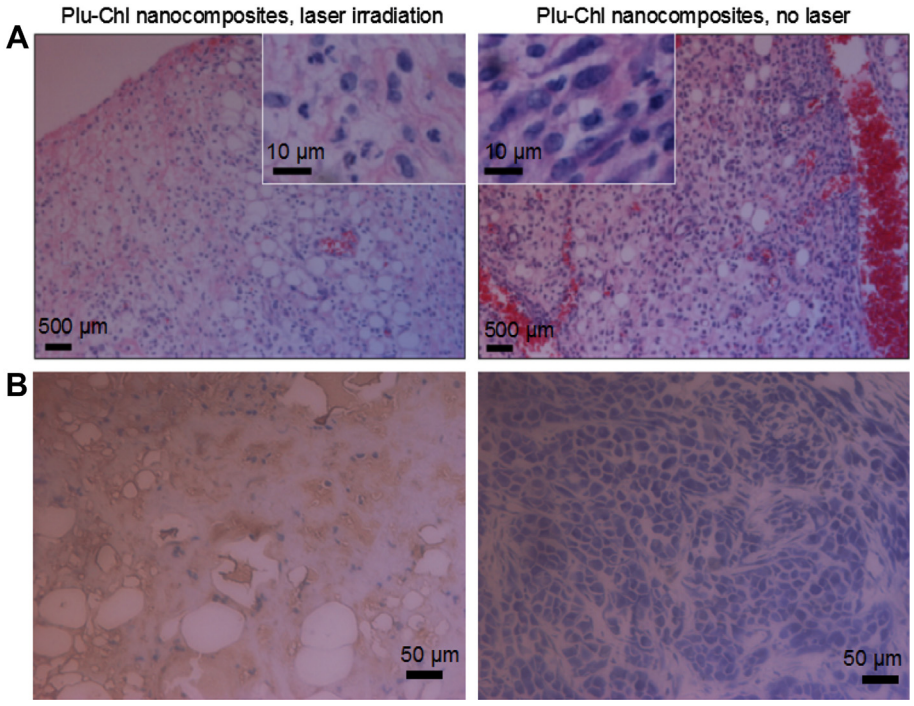

Fig. 15. Histologic assessments of mouse tumor tissues with and without photothermal therapy. (A) H&E stained images; (B) TUNEL assay images. The tumors were injected with PBS-dispersed Plu–Chl nanocomposites after 671-nm laser irradiation over 3 days (left panels) and without irradiation (right panels).

Acknowledgments

This work was supported in part by the National Natural Science Foundation of China (81071833, 31370961), the Nanoscience Foundation of Shanghai (13NM1402000) and the Program for New Century Excellent Talents in University (No. NCET-07-0618).

Appendix A. Supplementary material

Supplementary material associated with this article can be found, in the online version, at http://dx.doi.org/10.1016/j.biomaterials.2014.05.049.

References

[1] Peer D, Karp JM, Hong S, Farokhzad OC, Margalit R, Langer R. Nanocarriers as an emerging platform for cancer therapy. Nat Nanotechnol 2007;2:751–60.
[2] Fan L, Wu Q, Chu M. Near infrared fluorescent chlorophyll nanoscale liposomes for sentinel lymph node mapping. Int J Nanomed 2012;7:3071–80.
[3] Jubert C, Mata J, Bench G, Dashwood R, Pereira C, Tracewell W, et al. Effects of chlorophyll and chlorophyllin on low-dose aflatoxin B1 pharmacokinetics in human volunteers: a pilot study. Cancer Prev Res 2009;2:1015–22.
[4] Kensler TW, Qian GS, Chen JG, Groopman JD. Translational strategies for cancer prevention in liver. Nat Rev Cancer 2003;3:321–9.
[5] Lustig RA, Vogl TJ, Fromm D, Cuenca R, Hsi RA, D'Cruz AK, et al. A multicenter Phase I safety study of intratumoral photoactivation of talaporfin sodium in patients with refractory solid tumors. Cancer 2003;98:1767–71.
[6] Tsukaoshi S. Development of a novel photosensitizer, talaporfin sodium, for the photodynamic therapy (PDT). Gan to Kagaku Ryoho 2004;31:979–85.
[7] Brandis AS, Salomon Y, Scherz A. Chlorophyll sensitizers in photodynamic therapy. In: Grimm B, Porra R, Rüdiger W, Scheer H, editors. Chlorophylls and bacteriochlorophylls: biochemistry, biophysics, functions and applications25. Netherlands: Springer; 2006. pp. 461–83.
[8] Ulatowska-Jarża A, Zychowicz J, Hołowacz I, Bauer J, Razikc J, Wieliczko A, et al. Antimicrobial PDT with chlorophyll-derived photosensitizer and semiconductor laser. Med Laser Appl 2006;21:177–83.
[9] Gomaa I, Ali SE, El-Tayeb TA, Abdel-Kader MH. Chlorophyll derivative mediated PDT *versus* methotrexate: an *in vitro* study using MCF-7 cells. Photodiagnosis Photodyn Ther 2012;9:362–8.
[10] Lindsday CR, Lawn S, Campbell AD, Faller WJ, Rambow F, Mort RL, et al. P-Rex1 is required for efficient melanoblast migration and melanoma metastasis. Nat Commun 2011;2:555.
[11] Chu M, Pan X, Zhang D, Wu Q, Peng J, Hai W, et al. The therapeutic efficacy of CdTe and CdSe quantum dots for photothermal cancer therapy. Biomaterials 2012;33:7071–83.
[12] Huang X, El-Sayed IH, Qian W, El-Sayed MA. Cancer cell imaging and photothermal therapy in the near-infrared region by using gold nanorods. J Am Chem Soc 2006;128:2115–20.
[13] Huang P, Bao L, Zhang C, Lin J, Luo T, Yang D, et al. Folic acid-conjugated silica-modified gold nanorods for X-ray/CT imaging-guided dual-mode radiation and photo-thermal therapy. Biomaterials 2011;32:9796–809.
[14] Feng L, Wu L, Qu X. New horizons for diagnostics and therapeutic applications of graphene and graphene oxide. Adv Mater 2013;25:168–86.
[15] Yang HW, Liu HL, Li ML, Hsi IW, Fan CT, Huang CY, et al. Magnetic gold-nanorod/PNIPAAmMA nanoparticles for dual magnetic resonance and photoacoustic imaging and targeted photothermal therapy. Biomaterials 2013;34:5651–60.
[16] Ferruzzi M, Blakeslee J. Digestion, absorption, and cancer preventative activity of dietary chlorophyll derivatives. Nutr Res 2007;27:1–12.
[17] Chu M, Peng J, Zhao J, Liang S, Shao Y, Wu Q. Laser light triggered-activated carbon nanosystem for cancer therapy. Biomaterials 2013;34:1820–32.
[18] Gu L, Hall DJ, Qin Z, Anglin E, Joo J, Mooney DJ, et al. *In vivo* time-gated fluorescence imaging with biodegradable luminescent porous silicon nanoparticles. Nat Commun 2013;4:2326.
[19] Robertson CA, Abrahamse H, Evans D. The *in vitro* PDT efficacy of a novel metallophthalocyanine (MPc) derivative and established 5-ALA photosensitizing dyes against human metastatic melanoma cells. Lasers Surg Med 2010;42:766–76.
[20] Camerin M, Magaraggia M, Soncin M, Jori G, Moreno M, Chambrier I, et al. The *in vivo* efficacy of phthalocyanine-nanoparticle conjugates for the photodynamic therapy of amelanotic melanoma. Eur J Cancer 2010;46:1910–8.
[21] Borgul O, Kaplan M. Photodynamic therapy of dermal metastases of disseminated melanoma. Photodiagn Photodyn Ther 2012;9:S9–10.
[22] Kawczyk-Krupka A, Bugaja AM, Latosa W, Zarembac K, Sieroń A. Photodynamic therapy in treatment of cutaneous and choroidal melanoma. Photodiagn Photodyn Ther 2013;10:503–9.
[23] Dolmans DEJGJ, Fukumura D, Jain RK. Photodynamic therapy for cancer. Nat Rev Cancer 2003;3:380–7.
[24] Zhang M, Murakami T, Ajima K, Tsuchida K, Sandanayaka ASD, Ito O, et al. Fabrication of ZnPc/protein nanohorns for double photodynamic and hyperthermic cancer phototherapy. Natl Acad Sci U S A 2008;105:14773–8.

[25] Sahu A, Choi WI, Lee JH, Tae G. Graphene oxide mediated delivery of methylene blue for combined photodynamic and photothermal therapy. Biomaterials 2013;34:6239–48.
[26] Wang S, Huang P, Nie L, Xing R, Liu D, Wang Z, et al. Single continuous wave laser induced photodynamic/plasmonic photothermal therapy using photosensitizer-functionalized gold nanostars. Adv Mater 2013;25:3055–61.
[27] Kuo WS, Chang YT, Cho KC, Chiu KC, Lien CH, Yeh CS, et al. Gold nanomaterials conjugated with indocyanine green for dual-modality photodynamic and photothermal therapy. Biomaterials 2012;33:3270–8.
[28] Hirsch LR, Stafford RJ, Bankson JA, Sershen SR, Rivera B, Price E, et al. Nanoshell-mediated near-infrared thermal therapy of tumors under magnetic resonance guidance. Natl Acad Sci U S A 2003;100:13549–54.